A MODEL FOR PREDICTING THERMAL RADIATION HAZARDS FROM LARGE-SCALE LNG POOL FIRES

A.D. Johnson
Shell Research Ltd., Thornton Research Centre, P.O. Box 1, Chester CH1 3SH

A major accidental release of refrigerated liquefied natural gas (LNG) can ignite and form a large pool fire. This paper contains a description of a model for predicting the size and orientation of large-scale land-based LNG pool fires and the thermal radiation emitted to external objects. The model has been derived from measurements of experimental fires ranging in diameter from 1.8 m to 35 m. The computer program implementing the model has been designed to run quickly on a personal computer so that safety engineers can use it on a day-to-day basis.

KEYWORDS:
LNG Pool Fire Model, Thermal Radiation

INTRODUCTION

Natural gas is the world's third largest fossil energy reserve after coal and oil. Since 1960, more and more natural gas has been transported and stored as a refrigerated liquid - LNG. Considerable effort has been made to ensure the safe operation of LNG facilities and to understand the hazards consequent upon the accidental spillage of LNG.

One potential event following an accidental release of LNG is a pool fire, in which a large, bright, diffusion flame forms above a pool of vaporising LNG. The heat radiated from such large fires poses a significant hazard to nearby people and objects. The flame above a 35 m diameter pool of LNG on hard ground in a low wind would be approximately 70 m high and release some 6-7 Giga Watts of combustive power. Approximately 25% of this power would be emitted as thermal radiation.

Engineers, performing safety assessments on LNG facilities on a day-to-day basis, need quick and accurate methods of predicting the size, duration and radiative characteristics of LNG pool fires, to minimise the potential hazard to people and to design out the possibility of a fire damaging other plant or causing further escalation.

The processes governing the behaviour of LNG pool fires are extremely complex. The size of the flame depends upon the limitation of a feedback process linking fuel vaporisation and radiative heat transfer from the flame to the pool. The fire duration depends on the amount of liquid in the pool when it ignites, the mass consumption rate of the fuel - in turn governed by the heat feedback process, and on the time variation of the type of gas evolved from the pool. LNG pool fires undergo a fractional distillation process. Initially, the liquid temperature is close to that of boiling methane and methane is driven off; later, when most of the methane has evolved, the liquid temperature rises to the temperature of boiling ethane and ethane is driven off. The switch from methane to ethane evolution occurs within a few seconds, but at different times at different places in the pool.

In large-scale LNG pool fires, heat transfer is dominated by continuum radiation from incandescent soot. Soot production and oxidation is the most complex chemical process occurring within the flame. The chemical timescales are much longer than those of gaseous combustion and the chemistry cannot be separated from the turbulent flowfield. If soot escapes from the combusting gas envelope, it rapidly cools by radiative heat loss and thereafter blocks radiative heat transfer from within the flame to external objects.

Models that attempt to predict the fundamental thermo-chemical and fluid dynamical processes of LNG pool fires are only just being developed[1,2]. Such models are implemented as large numerical programs and take many hours to run on supercomputers. Moreover, soot chemistry, pool thermodynamics, and the modelling of turbulence generated by buoyancy are still very much in the realms of research.

The approach adopted over the last thirty years has been to model the principal phenomena using empirical correlations fitted to experimental measurements. The complex interaction between turbulent flow, chemistry and radiative heat transfer cannot be reproduced at laboratory scale, so experiments at a scale similar to the large fires of concern to safety engineers are required in order to produce reliable correlations.

Empirically based models are of varying complexity. The point source model is the simplest and is based on the assumptions that (a) the thermal radiation from a fire can be treated as coming from a point source, (b) the radiation decays as the inverse square of the distance from the source and (c) the radiant energy leaving the fire is a specified fraction of the energy released by combustion. Such models were used as part of the analysis of early LNG pool fire experiments by Burgess and Zabetakis[3] in 1962 and May and McQueen[4] in 1973.

Moorhouse and Pritchard[5] noted two limitations of point source models; the receiving surface is always assumed to be oriented so as to receive the maximum flux, and accurate prediction of heat flux to objects closer than about 5 pool diameters to the fire is not possible since in this region the relative geometry of the flame and receiving surfaces becomes important. In addition, there is generally no explicit allowance for the variation of radiation attenuation with atmospheric pathlength and most estimates of the fraction of combustive energy released as radiation (the F factor) are derived from laboratory experiments and are likely to be inaccurate since the dependence on scale is not understood.

Finally, there is evidence from the analysis of three 35 m diameter LNG pool fires[6], carried out at Montoir in Brittany in 1987 under the collaboration of British Gas, British Petroleum, Elf Aquitaine, Gaz de France, Shell and Total-CFP, that the radiation field from a large flame in a strong wind is not radially symmetric even at very large distances from a fire. When the flame is tilted and dragged downwind, it appears foreshortened from upwind and downwind viewpoints and wider from crosswind viewpoints. This asymmetry in the shape of the flame is reflected in the radiation field, and the radiation contours are not circular.

Surface emitter models (or solid flame models as they are sometimes known) were developed by Welker[7] and Atallah and Raj[8] for the analysis of American Gas Association sponsored land-based LNG fires in 1974. Surface emitter models replace the radiant gases and combustion products with a solid object which emits radiation from its surface. Markstein[9] observed that the radiant emission from the nonluminous parts of small propane diffusion flames is less than 10% of the emission from luminous flame. Narrow angle radiometer measurements from the sooty areas of the

35 m diameter Montoir fires confirm this view. Surface emitter models are therefore based on flame shapes that are fitted to the luminous flame envelope.

In this paper, a model of land-based LNG fires above circular or square pools is presented. The model describes the flame shape and thermal radiation for a steady fire under constant ambient conditions and when the flame is fuelled essentially by methane vapour. This stage of an LNG pool fire is considered to be most hazardous, since the flame is more smokey and less radiant in its later stages when it is fuelled by ethane. However, there may be a larger short-duration initial pulse of thermal radiation, which is hazardous to people, during the initial development of the flame. The flame shape is idealised as a tilted cylinder with an elliptic cross-section. The flame length, tilt from the vertical and downwind flame drag are described by empirical correlations derived from experimental fires ranging in diameter from 1.8 m to 35 m.

The flame is assumed to emit radiation uniformly from its surface and the total radiant power is correlated against pool diameter. The model includes an economical formula derived by Wayne[10] for calculating atmospheric attenuation of the infrared radiation emitted by the flame.

The simple geometric flame shape allows for the use of fast contour integration techniques, such as described by Davis and Bagster[11], when calculating the radiative heat transfer from the flame to an external receiving surface. The computer program implementing the model runs quickly enough on a personal computer for safety engineers to make predictions for safety assessments on a day-to-day basis.

THE THORNTON MODEL

In the Thornton model, the radiation flux q (kW/m^2) at a surface element outside the flame is given by:

$$q = VF\, S\, \tau \qquad \ldots (1)$$

where VF is the view factor,
S is the surface emissive power (SEP) in kW/m^2 and
τ is the atmospheric transmissivity, the fraction of emitted energy not absorbed or scattered by the atmosphere.

The view factor VF quantifies the geometric relationship between the model flame shape and receiving surfaces; it describes how much of the field of view of the receiving surface is filled by the flame. The view factor equals 1 if the flame completely fills the field of view of the receiving surface, otherwise it is a fraction of 1.

The flame shape parameters are found to depend on the pool diameter, and the direction and speed of the wind. Figure 1 shows the three basic parameters required to define the model flame shape, superimposed on a typical instantaneous cross-wind profile of an LNG pool fire flame.

S is an effective SEP, i.e. the SEP associated with the model flame shape in order to give the heat flux q specified in Equation (1). No attempt is made in this paper to relate this SEP to the actual surface emission from the flame, as would be measured by a narrow angle radiometer pointing at a small area of the surface of a real flame. S is in fact the total radiated power divided by the total model

flame area, including the base and the top. The total radiated power is found to depend on the pool diameter.

τ is an effective atmospheric transmissivity for all the paths through the atmosphere from points on the flame surface to the receiving surface. The atmospheric transmissivity τ is calculated using an efficient algorithm developed by Wayne[10]. The algorithm is based on the assumptions that the flame is a black body source at 1500 K, that CO_2 and H_2O are the only absorbing gases in the atmosphere and that atmospheric scattering is negligible. The transmissivity can be calculated for absorbing paths 10 to 1000 m long, through atmospheres of any relative humidity, at temperatures between 253 and 313 K.

The pathlength is taken in the model to be the distance from the receiving point to the model flame surface, along a line from the receiving surface to the geometric centre of the model flame. If the pathlength is less than 10 m, the transmissivity is set to 1.0. If the pathlength is greater than 1000 m, the value of the transmissivity for a pathlength of 1000 m is used instead.

EXPERIMENTS AND DATA ANALYSIS

The flame shape and total radiated power parameters are correlated against measurements from the large-scale experiments shown in Table 1. The LNG fires in Trials 1 and 4-9 were carried out in shallow bunds with floors of thermally insulating concrete so as to minimise the heat transfer to the pool from the substrate. The bunds in Trials 4,5 and 8 were also pre-cooled with liquid nitrogen to minimise the evaporation of methane during the filling of the bund. Trial 1 was carried out by Shell Research Ltd. Trials 2 and 3 were carried out by the American Gas Association in earthen bunds[7]. Trials 4 and 5 were carried out by British Gas[12]. Trials 6 and 7 were carried out jointly by British Gas and Shell Research Ltd. Trial 8 was carried out by Shell Research and was one of three 20 m diameter fires fuelled by LNG, refrigerated propane and kerosene[13]. Trial 9 was a collaborative effort by British Gas, British Petroleum, Elf Aquitaine, Gaz de France, Shell and Total-CFP[6].

For Trials 6-9, the measurements used in the flame shape correlations were obtained in the following manner. First, the experimental data was examined to identify periods when the ambient conditions were steady and the fire was fuelled by methane. Then, during each steady period, a tilted cylinder flame shape was superimposed by eye onto instantaneous crosswind images taken every 2 seconds from video. The length, tilt and drag of every instantaneous fit of the model flame shape were then used in deriving the model flame shape correlations. Data from the publications describing Trials 2, 3, 6 and 7, giving average values of the flame shape measurements, was also used in deriving the model flame shape correlations.

Mass burning rates were measured in Trials 4-9 using helium-purged dip-tubes which directly measured the liquid head. Only liquid regression rates were measured in Trials 2 and 3. Measurements of the liquid regression rates of the 35 m diameter fires, using arrays of thermocouples, indicate that it is very difficult to estimate the mass burning rate of LNG from a regression rate measurement, since the density of the LNG, which boils and foams below a fire, is not known.

In addition to visual records of each flame, ambient conditions and mass burning rate, measurements were made of the radiative heat flux from the flame to wide-angle radiometers, placed near ground level and facing toward the fire. Data was only used from those radiometers that received radiation from the whole of the visible flame. The average radiative heat flux was obtained for each period when the ambient conditions were steady.

MODEL CORRELATIONS

The mass burning rate was found to increase with pool diameter. Variations in wind velocity appeared to have no significant effect. The form of the mass burning rate correlation is the same as that suggested by Zabetakis and Burgess[14] and Welker[15] as a simplification of Hottel's[16] equation for heat transfer from a flame to a liquid pool. The mass burning rate is given by

$$\dot{m} = 0.141(1 - e^{-0.136D}) \text{ kg m}^{-2}\text{s}^{-1} \quad \ldots (2)$$

where D is the pool diameter in m.

The maximum mass burning rate of 0.141 kg $m^{-2}s^{-1}$ was obtained from the average measured mass burning rate from the 35m diameter fires in Trial 9. Flame emission spectra taken from bright areas of flame were very similar to those of black body emitters[6]; indicating that the radiative heat flux to the pool was unlikely to increase with further increase in pool diameter. Thus, 0.141 kg $m^{-2}s^{-1}$ is likely to be close to the maximum mass burning rate for a fire with negligible heat transfer from the substrate. The exponential coefficient was obtained by a least squares fit to data from Trials 6 and 7.

The correlation is plotted in Figure 2, along with the measurements from Trials 4-9. There is considerable scatter in the data, but the measurements from Trials 6 and 7 are close to the average of the mass burning rates measured by British Gas on square pools during Trials 4 and 5. The single measurement for a 20 m fire appears to be below average for a fire of that diameter.

The image analysis measurements of visible flame length vary considerably for nominally constant ambient conditions. The variation is partly owing to the difficulty of fitting the flat top of a cylindrical model flame shape to an ill-defined convoluted boundary, between bright flame and dark smoke, blurred by thinner layers of smoke. There is also an inherent time-dependent fluctuation in flame length caused by buoyancy driven instabilities in the flowfield and fluctuations in the windspeed. A correlation, derived by Moorhouse[12] for the length of cylindrical flame shapes fitted to images of LNG flames, was rejected because it underpredicted the average flame length in field trial 9, and because no dependency on windspeed could be determined.

Within the limitations of the tilted cylinder flame shape, the flame length L is adequately represented by Thomas's equation[17].

$$L = 42D\left[\frac{\dot{m}}{\rho_a (gD)^{1/2}}\right]^{0.61} \quad \ldots (3)$$

where $\dot{m}$ is the mass burning rate, given by equation (2),
ρ_a is the ambient density in kg/m^3 and
g is the acceleration due to gravity in m/s^2.

A new flame tilt correlation was derived, using image analysis measurements from Trials 2-9. The form of the correlation is similar to that derived by Welker and Sliepcevich[18]. The tilt from vertical θ is given by

$$\frac{\tan\theta}{\cos\theta} = 0.7(\text{Re})^{0.109}(\text{Fr})^{0.428} \quad \text{when } U > 0.4 \text{ m/s}$$
$$= 0 \quad \text{when } U < 0.4 \text{ m/s} \quad \ldots (4)$$

where Re is a Reynolds number given by

$$Re = (U\,D)/\nu_a$$

where U is the wind velocity in m/s,
ν_a is the kinematic viscosity of air in m^2/s

and Fr is a Froude number given by

$$Fr = U^2/(g\,D)\ .$$

The coefficients of the correlation were obtained by a linear least squares fit to the natural logarithms of the three dimensionless variables, Re, Fr and (tan θ/cos θ). The coefficients are similar to those derived by Moorhouse using data from smaller scale LNG pool fires[12]. The Welker and Sliepcevich correlation and Equation (4) are illustrated in Figure 3, together with the image analysis data. Although there is considerable scatter in the data, the correlation in Figure 3(a) is clearly a better fit than the correlation in Figure 3(b). The Froude number dependency is incorrect in the Welker and Sliepcevich correlation; the flame tilt is over predicted for high Froude numbers and under predicted for low Froude numbers. As a result, the root mean square difference between the measured flame tilt and the predicted flame tilt is 9.0 degrees for the Welker and Sliepcevich correlation and 6.8 degrees for the Thornton correlation.

A new correlation, describing the extent of downwind flame drag, was also derived using data from the 35 m, 20 m, and 10.6 m diameter fires. The length of the flame base D' is given by

$$\frac{D'}{D} = 1.49(Fr)^{0.0845} \quad \text{when } U > 0.4 \text{ m/s} \qquad ...(5)$$
$$= 1.0 \quad \text{when } U < 0.4 \text{ m/s}\ .$$

This correlation was obtained by a linear least squares fit to the natural logarithms of Fr and D'/D and is similar to one obtained by Moorhouse[12] using data from smaller diameter fires

$$\frac{D'}{D} = 1.5(Fr)^{0.069}\ . \qquad ...(6)$$

Figure 4 shows both correlations and the average and standard deviations of the flame drag measurements.

The correlation for the total radiated power was obtained in the following manner. Once the model flame shape correlations had been derived, the model flame shape was predicted for each period when the ambient conditions were steady. Then, Equation (1) was inverted, using all the valid average radiation heat fluxes to the wide-angle radiometers in Trials 1 and 6-9, to give the model SEP required to predict the radiation flux at each radiometer. It was assumed that the radiative heat flux through the top and bottom of the model flame shape was the same as through the sides; so the total radiated power was obtained by multiplying each calculated model SEP by the model flame surface area, including its base and top.

Next, it was assumed that the total radiated power from an LNG flame is constant at a given pool diameter. This assumption was justified by the fact that no significant difference could be discerned from test to test between the predictions from the radiometers in the three 35 m diameter tests in Trial 9, even though the test conditions varied greatly. A systematic difference was noted between

calculated total radiated powers from radiometers in a given test however, indicating that the SEP varies azimuthally around a flame. However, this simple model can only cope with a uniform SEP for the modelled flame.

The correlation for the total radiated power is given by

$$\frac{\text{Total Radiated Power}}{\pi D^2/4}\ (kW/m^2) = 2.26\times10^3(1 - e^{-0.153D}) \quad D < 11m \qquad ...(7)$$
$$= 2.26\times10^3(1 - e^{-0.153D})e^{-0.012(D-11)} \quad D > 11m$$

The mean calculated total radiated power, divided by the pool area, is plotted in Figure 5 against pool diameter with an error bar of one standard deviation of the data about the mean. The data points indicate that the total radiated power per unit pool area increases to a maximum at a pool diameter of about 20 m and thereafter decreases with increasing pool diameter. The solid line is the correlation which is a least squares fit to the mean values of total radiated power per unit pool area.

The form of the correlation is suggested by the following physical reasoning. As the pool diameter increases from zero, more and more soot is produced because there is less aeration. For pool diameters less than about 10 m, this soot is hot and incandescent and the radiation contribution from the hot soot increases with pool diameter. The total radiated power per unit pool area thus increases with pool diameter. However, at pool diameters greater than 10 m, soot begins to escape from the flame before it is completely burnt. This soot cools rapidly and instead of radiating heat, absorbs strongly, thereby reducing the radiation leaving the fire to points outside. The increase of dark soot leaving the flame also indicates a loss of combustion and radiation efficiency. Thus, the total radiated power per unit pool area begins to decrease with increasing pool diameter. The same behaviour is noted for heavier hydrocarbon pool fires but the decrease begins at a smaller scale.

In the Thornton model, the SEP used in Equation (1) is calculated by dividing the total radiated power predicted by Equation (7) by the total area of the model flame shape given by Equations (3) - (5).

VIEW FACTOR CALCULATION

The view factor VF in Equation (1), for a differential oriented receiving surface, is derived from the application of Lambert's cosine rule[19] and is given by

$$VF = \iint_R \frac{\cos\theta_1 \cos\theta_2}{\pi r^2}\, dA_1\ , \qquad ...(8)$$

where R is the part of the model flame surface (A_1) that is visible from the differential oriented receiving element dA_2,
r is the distance along a line from the receiving element dA_2 and a differential area element dA_1 of the flame,
θ_2 is the angle between the normal to dA_2 and that line and
θ_1 is the angle between the local normal to the surface at dA_1 and that line.

A typical flame-receiving surface configuration is shown in Figure 6. The surface R is formed by the set of points on the model flame surface for which $\cos\theta_1$ and $\cos\theta_2$ are greater than zero.

Equation (8) involves the surface integration of a complex geometrical function. This calculation is the most time-consuming part of any radiation hazard prediction using a surface emitter model. Analytical solutions have been found for certain model flame shapes and receiver orientations[20, 21]. For general locations and orientations of the receiving surface and for more complicated model flame shapes, it has been necessary to evaluate Equation (8) numerically[22, 23].

Sparrow and Cess[24] have described how, using Stokes's theorem, Equation (8) can be reduced from an integral over the surface R to a contour integral around the boundary of R, shown by the thick line in Figure 6. This approach is adopted in the Thornton model and is implemented in a similar way to that reported by Davis and Bagster[11].

Often however, it is the prediction of the maximum heat flux at a point outside the flame that is required, rather than the flux to a surface of known orientation. The maximum flux is required, for instance, when predicting the radiation fluxes to personnel, or to plant with complex geometries, where it is likely that some part of the receiving surface is oriented so as to receive the maximum radiative heat flux. At a given point outside the flame, the radiative heat flux given by Equation (1) is at a maximum when the view factor is at a maximum.

For a tilted cylinder model flame shape, it can be shown that the maximum view factor VF_{max} is given by:

$$VF_{max} = (VF_x^2 + VF_y^2 + VF_z^2)^{1/2} \quad \ldots (9)$$

where each of the variables VF_x, VF_y and VF_z is given by a surface integral similar to Equation (8)

$$VF_x, VF_y \text{ or } VF_z = \iint_{R_{max}} \frac{\text{Cos } \theta_1 \text{ Cos } \theta_2}{\pi r^2} \, dA_1 \quad , \quad \ldots (10)$$

where, for VF_x, VF_y and VF_z the differential receiving element dA_2 is located at the receiving point with its normal pointing in the x, y and z direction, respectively.

However, an important difference from Equation (8), is that the surface R_{max} is formed by the set of points on the model flame surface for which only Cos θ_1 is greater than zero. R_{max} is thus the maximum model flame surface visible from the receiving point.

In the Thornton model, contour integration techniques have been implemented to evaluate Equation (10) when calculating maximum view factors.

Using contour integration, rather than numerically evaluating the surface integrals, the time taken to generate radiative heat flux values across a typical 45 x 30 grid (1350 points), for later contour plotting, has been reduced from 20 minutes to approximately 2 minutes, using RM/FORTRAN on an IBM PS/2 with a maths coprocessor.

COMPARISON OF PREDICTED RADIATION LEVELS WITH MEASURED VALUES

The calculated radiation levels and flame parameters are compared with measured values in Tables 2-4. In addition, Figure 7 shows calculated radiation heat flux contours compared with ground level contours obtained from measurements during the second 35 m diameter Montoir fire[6]. The

calculations cover a wide range of pool sizes (1.8 m - 35 m) and wind speeds (2.4 m/s - 9.6 m/s). The agreement between the calculated and measured radiation heat fluxes is good, generally the calculations lie within one standard deviation of the average measured heat flux, and most calculated values lie within 10% of the measured mean.

The calculated flame tilts are also in good agreement with the measured values, again lying within the standard deviation of the measured tilts and within 10% of the average measured values for Trials 1 and 6. The Welker and Sliepcevich correlation, shown in Figure 3(b), predicts tilts of 56 degrees for Trial 1, 66 degrees for Trial 6 and 45 degrees for Trial 7.

The radiation heat fluxes measured by radiometers 9 and 10 in Table 3, placed directly upwind of the pool and close to the pool, are noticeably higher than the calculated values. Measurements of infrared emission spectra show that the radiative emission is not saturated for a 6.1 m diameter LNG pool fire, and the emission increases with increasing pathlength through the flame. The flame in this test was considerably tilted and dragged by the wind. As a consequence, much of the heat flux received at radiometers 9 and 10 came from radiating paths that were longer and hence had higher radiative emissions than radiating paths through the flame in the crosswind direction. This azimuthal variation of the emitted radiation cannot be predicted by the model described in this paper, because it is based on the assumption of uniform surface emission.

The contours in Figure 7 are not circular, even at a distance of nearly 6 pool diameters from the pool centre. This shows that, for large highly wind-tilted flames, the relative geometry of the flame and receiving surfaces is important, even in the far field. A point source model, which predicts circular radiation contours, would not give good predictions of the radiation field in this case.

CONCLUSIONS

1. The radiation field around land-based LNG pool fires is well described by a model in which the flame is idealised as a surface emitter in the shape of a tilted cylinder with an elliptical cross-section.

2. Compared with point source radiation models, the surface emitter model has a firmer theoretical basis and more realistic geometrical representation. The radiation field around large, highly wind-tilted flames does not approximate to the radiation from a point source, even far away from the flame.

3. The empirical correlations used in the Thornton model have been fitted to experimental data obtained from a wide range of test conditions. The accuracy of radiation predictions is sufficient to provide a reliable basis for safety assessments.

4. Experimental tests have shown that the radiative power per unit pool area of land-based LNG pool fires increases with increasing pool diameter until the pool diameter reaches about 20 m, thereafter, it decreases with increasing pool diameter.

5. Fast contour integration techniques for evaluating the oriented and maximum view factors have been used in the Thornton model so that radiative heat flux predictions can be produced quickly on a personal computer.

NOMENCLATURE

A_1	Model flame surface
dA_1	Differential element of the model flame surface
dA_2	Differential receiving surface
D	Pool diameter, m.
Fr	Froude number.
g	Acceleration due to gravity, m/s^2.
L	Flame length, m.
$\dot{m}$	Mass burning rate, kg $m^{-2}s^{-1}$.
r	Distance from differential element of model flame surface to differential receiving surface.
Re	Reynolds number.
S	Model surface emissive power, kW/m^2.
SEP	Surface emissive power, kW/m^2.
U	Ambient windspeed, m/s.
VF	View factor or configuration factor.
VF_{max}	Maximum view factor
VF_x	Contribution to maximum view factor from surface oriented with normal pointing in the x-direction.
VF_y	Contribution to maximum view factor from surface oriented with normal pointing in the y-direction.
VF_z	Contribution to maximum view factor from surface oriented with normal pointing in the z-direction.
θ	Flame tilt from the vertical.
θ_1	Angle between the normal to a point on the flame surface and a line from the point on the flame to the receiving surface.
θ_2	Angle between the normal to the receiving surface and a line from the point on the flame to the receiving surface.
ν_a	Kinematic viscosity of air, m^2/s.
ρ_a	Air density, kg/m^3.
τ	Atmospheric transmissivity.

REFERENCES

1. Borghi R., Coppalle A., Lecossais E. and Bauer B., 1989, "Measurements of LNG Pool Fires radiative properties and theoretical calculations", Euromech Colloquium 249 on plumes and turbulent jet diffusion flames in the atmosphere, 22-25 May, Madrid.
2. Most J.M. and Joulain P., 1990, "Numerical Models and Experimental Validation of Turbulent Diffusion Flames", Proc. Eurotherm Seminar Nr. 14, Session V, 15-17th May, Louvain-la-Neuve, Belgium.
3. Burgess D.S and Zabetakis M.G., 1962, "Fire and explosion hazards associated with LNG", US Bureau of Mines Report 6099.
4. May W.G. and McQueen W., 1973, "Radiation from Large Liquefied Natural Gas Fires", Combustion Science and Technology, 7, pp.51-56.
5. Moorhouse J. and Pritchard M.J., 1982, "Thermal Radiation Hazards from Large Pool Fires and Fireballs - A Literature Review", I. Chem. E. Symp. Series No. 71.
6. Nedelka D, Moorhouse J and Tucker R.F., 1989, "The Montoir 35m Diameter LNG Pool Fire Experiments", TRCP.3148R, presented at 9th Int. Congress and Exposition of Liquefied Natural Gas, "LNG9", 17-20 October, Nice, France.

7. Welker J.R., 1974, "Radiant Heating from LNG Fires", AGA report IS-3-1, Section F.
8. Atallah S. and Raj P.P.K., 1974, "Radiation from LNG Fires", AGA report IS-3-1, Section G.
9. Markstein G.H., 1976, "Scaling of Radiative Characteristics of Turbulent Diffusion Flames", 16th Int. Symp. on Comb. p.1402.
10. Wayne F.D., 1991, "An Economical Formula for Calculating Atmospheric Infrared Transmissivities", J. Loss Prev. in Process Industries, 4, No.2, pp86-92.
11. Davis B.C. and Bagster D.F., 1989, "The Computation of View Factors of Fire Models", J. Loss Prev. Process Ind. 2, pp.224-234.
12. Moorhouse J, 1982, "Scaling laws for Pool Fires determined from Large Scale Experiments" I. Chem. E. Symposium series, No. 71, pp.165-179.
13. Mizner G.A. and Eyre J.A., 1982, "Large-Scale LNG and LPG Pool Fires" I. Chem. E. Symposium series, No. 71, pp.147-163.
14. Zabetakis M.G. and Burgess D.S, 1961, "Research in Hazards Associated with the Production and Handling of Liquid Hydrogen", US Bureau of Mines Report, RI5707.
15. Welker J.R., May, 1974, "Predict LNG fire Radiation", Hydrocarbon Processing, pp.141-143.
16. Hottel H.C., 1959, "Certain Laws Governing Diffusive Burning of Liquids", Fire Reserach Abstr. Rev. 1, p.41.
17. Thomas P.H., 1963, 9th Int. Combustion Symp. Comb. Inst. Pittsburg, PA, USA, p.844.
18. Welker J.R. and Sliepcevich C.M., 1966, Fire Technology, 2, p.127.
19. Hottel H.C. and Sarofim A.F., 1967, "Radiative Transfer", McGraw-Hill, New York.
20. Raj P.P.K., May 1977, "Calculations of Thermal Radiation Hazards from LNG Fires - A Review of the State of the Art", Paper 2, AGA Transmission Conference, St Louis, USA.
21. Mudan K.S., 1987, "Geometric View Factors for Thermal Radiation Hazard Assessment", Fire Safety Journal, 12, pp.89-96.
22. Rein R.G., Sliepcevich C.M. and Welker J.R., 1970, "Radiation View factors for Tilted Cylinders", J. Fire and Flammability, 1, pp 140-153.
23. Hankinson G., October, 1985, "A Method for Calculating the Configuration Factor between a Flame and a Receiving Target for a Wide Range of Flame Geometries Relevant to Large Scale Fires", Fire Safety Sciences, First International Symposium.
24. Sparrow E.M. and Cess R.D., 1978, "Radiation Heat Transfer", McGraw Hill Book Company, New York.

TABLE 1 - Ranges of parameters covered by LNG pool fire tests

Trial number m	Pool diameter m/s	Wind speed °C	Ambient temperature %	Relative humidity mbar	Ambient pressure	Other	No. of tests
1	1.8	2.4	-	-	-	-	1
2	1.8	1.5 - 5.9	15 - 26	39 - 51	-	soil dykes	6
3	6.1	3.1 - 6.9	22 - 23	41 - 66	-	soil dykes	6
4	6.1 x 6.1	1.8 = 13.5	-	-	-	liquid N_2 pre cooled	10
5	12.2 x 12.2	2.2 - 13.5	-	-	-	liquid N_2 pre cooled	5
6	6.1	5.4 - 9.7	7	83	943	-	1
7	10.6	3.7 - 6.3	9	87	943	-	1
8	20	5.4 - 7.5	27	53	-	liquid N_2 pre cooled	1
9	35	2.7 - 10.1	14 - 25	53 - 85	1009 - 1022		3

(- indicates data not available)

TABLE 2 - Comparison of calculated radiation levels with measured values
1.8m diameter fire - Field trial 1

Radiometer number	Location			Radiation			
	X (m)	Y (m)	Z (m)	PHI (deg)	THETA (deg)	Calculated (KW/m^2)	Measured (KW/m^2) Avg. Std.dev
1	1.09	-6.20	1.0	260.0	90.0	4.61	4.77 0.63
2	-2.15	-5.92	1.0	290.0	90.0	4.31	4.22 0.48
3	4.05	-4.83	1.0	230.0	90.0	3.61	2.99 0.29
4	5.92	-2.15	1.0	200.0	90.0	2.77	2.62 0.34
5	6.20	1.09	1.0	270.0	90.0	2.14	1.91 0.23

Ambient conditions		Flame parameters		
			Calculated	Measured Avg. Std.dev
Air temperature, °C	-	Flame length, m	3.31	-
Air pressure, bar	-	Flame tilt, deg.	48.6	47.5 6.5
Relative humidity, %	-	Flame drag ratio	1.35	-
Wind speed, m/s	2.4	Mass burning rate, kg m^{-2} s^{-1}	0.03	
Wind direction, Clockwise from North	270.0	SEP, kW m^{-2}	56.1	

(- indicates data not available)

(Note that the air temperature, pressure and relative humidity are not important for this test since the atmospheric pathlengths are less than 10m and the model neglects atmospheric absorption of radiation)

Coordinate system for Tables 2-4

The coordinate system for the location and orientation of the radiometers and the wind direction is as follows: The origin is the centre of the pool; the X-axis points North; the Y-axis points West; the Z-axis points vertically upwards; PHI is the angle that the horizontal projection of the normal to the radiometer receiving surface makes with the positive X-axis, measured clockwise from the X-axis; and THETA is the angle from the vertical to the normal to the radiometer receiving surface. The wind direction is the direction from which the wind is blowing, measured clockwise from the positive X-axis.

TABLE 3 - Comparison of calculated radiation levels with measured values
6.1m diameter fire - Field trial 6

Radiometer number	Location					Radiation		
	X (m)	Y (m)	Z (m)	PHI (deg)	THETA (deg)	Calculated (KW/m^2)	Measured (KW/m^2) Avg.	Std.dev
1	28.0	0.0	1.07	180.0	90.0	3.03	2.77	0.72
2	33.0	0.0	1.07	180.0	90.0	2.17	2.13	0.52
3	16.5	-28.58	1.07	240.0	90.0	3.39	2.73	0.29
4	21.0	-36.37	1.07	240.0	90.0	1.62	1.57	0.19
5	0.0	-25.0	1.07	270.0	90.0	7.57	5.65	0.93
6	0.0	-33.0	1.07	270.0	90.0	3.24	3.07	0.42
7	0.0	-38.0	1.07	270.0	90.0	2.14	1.99	0.26
8	0.0	-42.0	1.07	270.0	90.0	1.61	1.32	0.35
9	0.0	15.0	1.07	90.0	90.0	3.45	5.09	0.58
10	0.0	18.0	1.07	90.0	90.0	2.58	3.12	0.37
11	0.0	25.0	1.07	90.0	90.0	1.51	1.34	0.35
12	12.5	21.65	1.07	120.0	90.0	1.95	1.94	0.25
13	16.5	28.57	1.07	120.0	90.0	1.21	1.26	0.16

Ambient conditions		Flame parameters		
			Calculated	Measured Avg. Std.dev
Air temperature, °C	7.0	Flame length, m	14.3	-
Air pressure, bar	0.943	Flame tilt, deg.	58.2	57.4 6.6
Relative humidity, %	83.0	Flame drag ratio	1.45	-
Wind speed, m/s	6.6	Mass burning rate, kg m^{-2} s^{-1}	0.079	0.085
Wind direction, Clockwise from North	250.0	SEP, kW m^{-2}	122.6	

(- indicates data not available)

TABLE 4 - Comparison of calculated radiation levels with measured values
10.6m diameter fire - Field trial 7

Radiometer number	Location					Radiation		
	X (m)	Y (m)	Z (m)	PHI (deg)	THETA (deg)	Calculated (KW/m^2)	Measured (KW/m^2) Avg.	Std.dev
1	38.0	0.0	1.25	180.0	90.0	5.40	5.58	0.61
2	48.0	0.0	1.25	180.0	90.0	3.56	4.52	0.51
3	56.0	0.0	1.25	180.0	90.0	2.67	2.91	0.42
4	46.76	-27.0	1.25	210.0	90.0	2.21	2.28	0.2
5	16.5	-28.58	1.25	240.0	90.0	3.98	3.43	0.24
6	21.0	-36.37	1.25	240.0	90.0	2.69	2.77	0.25
7	25.0	-43.3	1.25	240.0	90.0	2.01	2.22	0.22
8	0.0	-33.0	1.25	270.0	90.0	3.60	3.67	0.33
9	0.0	-38.0	1.25	270.0	90.0	2.87	2.92	0.27
10	0.0	-50.0	1.25	270.0	90.0	1.81	1.42	0.31
11	0.0	48.0	1.25	90.0	90.0	7.12	5.36	0.53
12	0.0	56.0	1.25	90.0	90.0	4.62	3.93	0.33
13	0.0	63.5	1.25	90.0	90.0	3.26	3.03	0.61

Ambient conditions		Flame parameters		
			Calculated	Measured Avg. Std.dev
Air temperature, °C	9.3	Flame length, m	25.3	-
Air pressure, bar	0.943	Flame tilt, deg.	47.1	42.2 7.1
Relative humidity, %	87.0	Flame drag ratio	1.27	1.48 0.14
Wind speed, m/s	4.0	Mass burning rate, kg m^{-2} s^{-1}	0.108	0.105 to 0.107
Wind direction, Clockwise from North	90.0	SEP, kW m^{-2}	158.1	

(- indicates data not available)

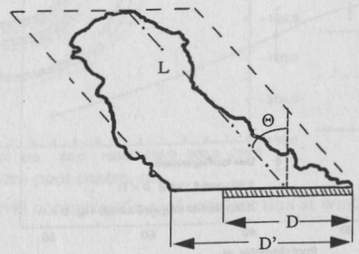

FIG. 1 - Model flame shape parameters superimposed on instanteneous LNG flame profile

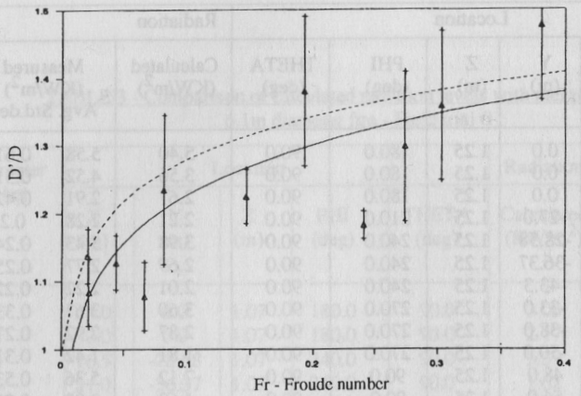

FIG. 4 - Flame drag correlation

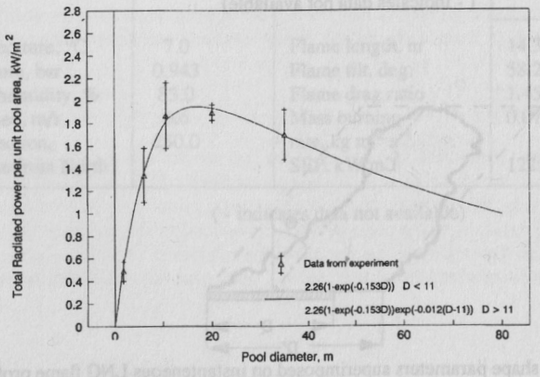

FIG. 5 - Total radiated power correlation

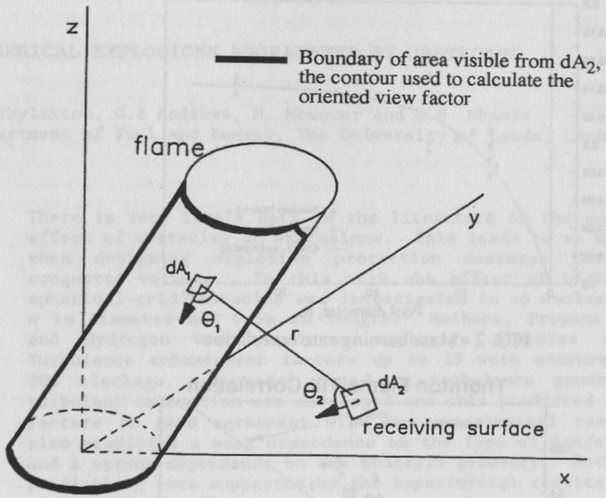

FIG. 6 - Typical configuration of a flame and receiving surface

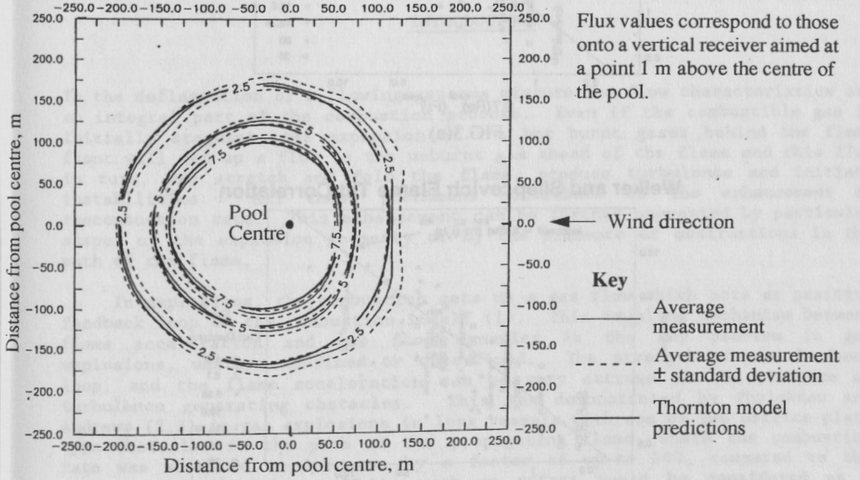

Flux values correspond to those onto a vertical receiver aimed at a point 1 m above the centre of the pool.

FIG. 7 - Ground level contours of equal incident flux at wind speed of 9.6 m/s

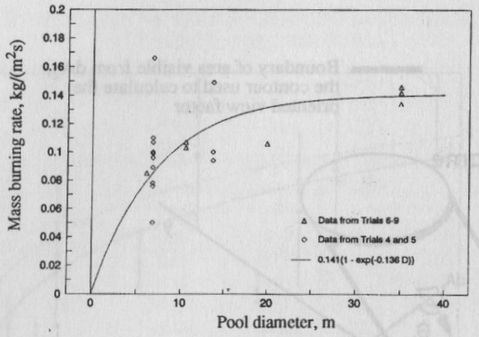

FIG. 2 - Mass burning rate correlation

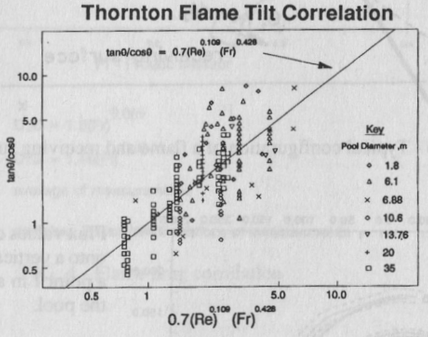

FIG.3(a)

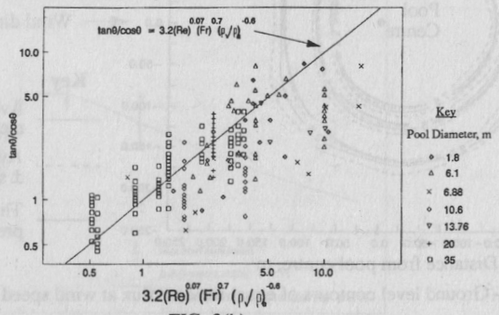

FIG. 3(b)

FIG. 3 - Flame tilt correlation

SPHERICAL EXPLOSIONS AGGRAVATED BY OBSTACLES

H. Phylaktou, G.E Andrews, N. Mounter and K.M. Khamis
Department of Fuel and Energy, The University of Leeds, Leeds LS2 9JT

There is very little data in the literature on the quantitative effect of obstacles on explosions. This leads to an uncertainty when designing explosion protection measures for obstacle congested volumes. In this work the effect of high-blockage, spherical-grid obstacles was investigated in an enclosure of 0.5 m in diameter and 0.5m in length. Methane, Propane, Ethylene and Hydrogen were used as explosive mixtures with air. Turbulence enhancement factors up to 15 were measured with an 80% blockage. A model based on turbulence generation and turbulent combustion was developed and this predicted turbulence factors in good agreement with the experimental results. It also predicted a weak dependence on the type of gas/air mixture and a strong dependence on the obstacle geometry. Both of these predictions were supported by the experimental results.

Key Words: Spherical Explosions, Obstacles, Turbulence Factor, Model.

INTRODUCTION

In the deflagration of a flowing gaseous mixture the flow characteristics are an integral part of the combustion process. Even if the combustible gas is initially stagnant, the expansion of the hot burnt gases behind the flame front will set up a flow in the unburnt gas ahead of the flame and this flow in turn, may stretch and fold the flame, produce turbulence and initiate instabilities. All these phenomena contribute to the enhancement of thecombustion rate. This enhancement can be further augmented by particular shapes of the explosion geometry or by the presence of obstructions in the path of the flame.

In explosions, the combustion sets up a gas flow which acts as positive feedback loop on the combustion itself (1). This coupling mechanism between flame acceleration and gas flow dynamics is the key problem in gas explosions, whether confined or unconfined. The strength of the feedback loop, and the flame acceleration can be very extreme in the presence of turbulence generating obstacles. This was demonstrated by Phylaktou and Andrews (2,3) in gas explosions in long vessels with one or two orifice-plate type obstacles in the path of the propagating flame, where the combustion rate was measured to increase by a factor of up-to 200, compared to the unobstructed explosion. While such an effect would be considered as a beneficial enhancement in a controlled combustion process, and indeed turbulent burning is the normal mode of operation in many combustion systems, it can not be considered as an 'enhancement' in an accidental explosion scenario. Obstacles have rather an aggravating effect on an explosion; they